Alma Mater Studiorum · Università di Bologna

Dipartimento di Fisica e Astronomia "Augusto Righi"
Corso di Laurea in Fisica

Event reconstruction and selection performances of KM3NeT/ORCA and comparison with KM3NeT/ARCA

Relatore:
Prof. Maurizio Spurio

Presentata da:
Luigi Lemma

Correlatori:
Dott.ssa Ilaria Del Rosso
Dott.ssa Giulia Illuminati

Anno Accademico 2024/2025

Abstract

Solo in tempi recenti abbiamo iniziato a studiare l'impatto che il neutrino potrebbe avere nei campi dell'astronomia. Questa particella elusiva interagisce con la materia ordinaria con piccola probabilità solo via interazione debole, rendendolo un ideale portatore di informazioni della sua sorgente. Per di più, il suo cammino non viene deflesso da campi magnetici, ciò ci permette di tracciare la posizione della sorgente nel cielo.

Nel corso degli ultimi anni, vasti telescopi sono stati costruiti sott'acqua per la rilevazione del neutrino. Due fra questi sono KM3NeT/ORCA e KM3NeT/ARCA, situati rispettivamente a largo della costa di Tolone e della Sicilia. L'obiettivo del primo è collezionare dati in merito al meccanismo di oscillazione dei neutrini, il secondo è invece usato per raccogliere informazioni riguardo determinate sorgenti astrofisiche. Per riuscirci questi telescopi utilizzano la radiazione Cherenkov indotta nel mezzo dal passaggio delle particelle cariche prodotte dalle interazioni di neutrini.

In questo lavoro si presenta una serie di risultati al fine di valutare le prestazioni del rivelatore per la rivelazione di neutrini. In particolare, tali esiti riguardano la contaminazione muonica di KM3NeT/ORCA e KM3NeT/ARCA, oltre che le loro risoluzioni angolari e energetiche e le loro aree efficaci. Spettri energetici diversi sono stati considerati ai fini del confronto tra prestazioni.

Table of Contents

Chapter 1

Neutrino Astronomy

1.1 Historical background

In the early 1900s, decays were categorized in three different types based on their products' ability to penetrate matter: α, β and γ. Each of them represents a specific particle as a result of the interaction, namely α-decays have as one of their products an Helium nucleus (α particle), β-decays an electron (β particle) and γ-decays a photon (γ particle). From the theory of special relativity we know that in a two body decay problem the final energy must be discrete, this was experimentally confirmed in α-decays and γ-decays but not in β-decays of the form:

$$ {}^{A}_{Z}X \rightarrow {}^{A}_{Z+1}X + \beta \tag{1.1} $$

which showed instead a continuous energy spectrum.
Following these observations, during the 30s Wolfgang Pauli hypothesized the existence of a third reaction's product, a fermionic particle, in order to satisfy the conservation of angular momentum, with neutral electric charge and no mass. Afterwards, Enrico Fermi named this hypothesized particle neutrino, considering its elusive nature. In 1956, the existence of the neutrino was confirmed by the Cowan-Reines experiment observing fission fragments resulting from the β^{-}-decays.

1.2 Introduction to neutrino physics

In the Standard Model (SM) the neutrino is characterized as a particle of half-integer spin with no electrical or color charge and no mass; it belongs to the category of the neutral leptons. The neutrino interacts then only via weak interaction. Leptons are further divided in three different flavours, based on each charged lepton: electron (e^-), muon (μ^-) and tau (τ^-). There is a neutrino associated to each flavour, respectively: electron neutrino (ν_e), muon neutrino (ν_μ) and tau neutrino (ν_τ). The SM predicts that to each charged lepton it is associated an opposite charged lepton, to which we refer to as antilepton. The corresponding neutrinos are then called antineutrinos.

1.2.1 Weak interaction

It constitutes one of the known four fundamental forces, weaker than strong and electromagnetic interaction but stronger than the gravitational one. It mediates the decay or interaction processes through a set of three particles: the $W^\pm$ bosons, which mediate Charged Current or CC processes, and the Z^0 boson, which mediates Neutral Current or NC processes. Each interaction is classified as *leptonic* or *hadronic*, whether just leptons or hadrons take part to the reaction; if both leptons and hadrons are involved we call the interaction *semi-leptonic*.

A typical leptonic interaction is the muon decay:

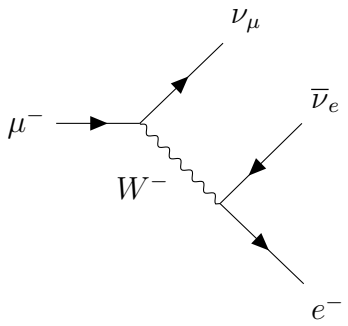

Figure 1.1: Feynman diagram of a muon decay, on Earth often occurring in the atmosphere. The horizontal axis represents time while the vertical axis represents space.

As we can see in figure 1.1, the muon decay is a CC process mediated by the W^- boson, resulting then in a change of the products flavour. In particular, a lepton flavour quantum number is associated to each lepton and antilepton of the same family taking part in the decay, being equal to +1 and -1 respectively. It has never been observed a violation of the conservation of such quantum number during interaction or decay processes.

1.2.2 Neutrino oscillation

During the 60s Bruno Pontecorvo, after better specified by Maki, Nakagawa e Sakata, hypothesized the possibility for neutrinos to change flavour in flight, a phenomenon known as neutrino oscillation. Each flavour is associated with either one of the states ν_e, ν_μ and ν_τ, known as flavour eigenstates. As neutrinos propagates through the Universe, one has to consider the mass eigenstates ν_1, ν_2 and ν_3, instead of the flavour eigenstates. In order to discuss the mass-oscillation relation, we need to use a quantum mechanical approach, defining the flavour eigenstates as follows:

$$|\nu_f\rangle \ , \ \text{with} \ f \in \{e, \mu, \tau\} \tag{1.2}$$

and the mass eigenstates, associated to a mass observable:

$$|\nu_i\rangle \ , \ \text{with} \ i \in \{1, 2, 3\} \tag{1.3}$$

In the void, flavour and mass eigenstates can be considered as linearly dipendent and a relation between the two can therefore be derived:

$$|\nu_f\rangle = \sum_i U_{fi} \, |\nu_i\rangle \tag{1.4}$$

Where U_{fi} are elements of the so-called *mixing* or Pontecorvo-Maki-Nakagawa-Sakata (PMNS) matrix.

The flavour eigenstates must be separated from those of mass. It is required for the U_{fi} elements and the mass eigenvalues m_i of neutrinos to take non-zero values; m_i must also be non-degenerate.

1.3 Neutrino Sources

Neutrinos are produced in large quantities in our cosmos, different types of sources emit these particles with different energy spectra.

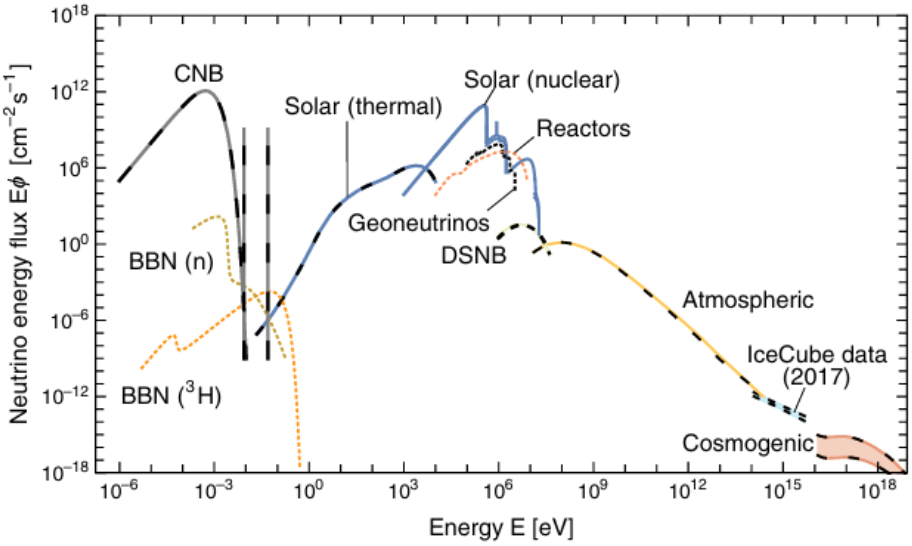

Figure 1.2: Neutrino energy flux at Earth, integrated over directions and summer over flavours. Solid lines are used for neutrino (ν), dashed lines are used for antineutrino ($\bar{\nu}$) and superimposed dashed and solid lines are used for both ν and $\bar{\nu}$ [1].

The various graphs in figure 1.2 show different contributes to the neutrino energy flux ($E \times \Phi$) at Earth, with Φ being the neutrino flux, i.e., the number of neutrinos per unit square centimeter per unit second per unit energy at Earth. The most intense hypothesized sources, for emitted neutrinos that reach our planet, are the cosmic neutrino background (CNB), less energetic ($E \sim$ meV), and the Sun, more energetic ($E \sim$ MeV).

1.3.1 Solar neutrinos

The amount of neutrinos from the Sun only that reach the Earth every second per square centimeter is on average $6 \times 10^{10}\,\mathrm{s^{-1}cm^{-2}}$. The previous estimate is the result of the following approximate expression for the solar neutrino energy flux:

$$\Phi_{\nu_e} \approx \frac{1}{4\pi D_\odot^2}\frac{2L_\odot}{Q}\,, \quad with\ Q = 26.73\,\mathrm{MeV} \tag{1.5}$$

where $D_\odot$ and $L_\odot$ are respectively the average distance between the Sun and the Earth and the solar luminosity.

The first evidence of solar neutrino comes from the Homestake experiment [2] where it has been used the following relation to measure the neutrino flux:

$$\nu_e + {}^{37}Cl \rightarrow e^- + {}^{37}Ar \tag{1.6}$$

Of all the Sun reactions the thermonuclear ones produce the largest amount of neutrinos. They happen because of the nuclear fusion, occurring in the Sun's core, via two main processes: the pp chain and the CNO cycle. They both rely on the following equation [3]:

$$4p \rightarrow {}^4He + 2e^+ + 2\nu_e + Q \tag{1.7}$$

A distribution of the contributions deriving from each cycle is shown below:

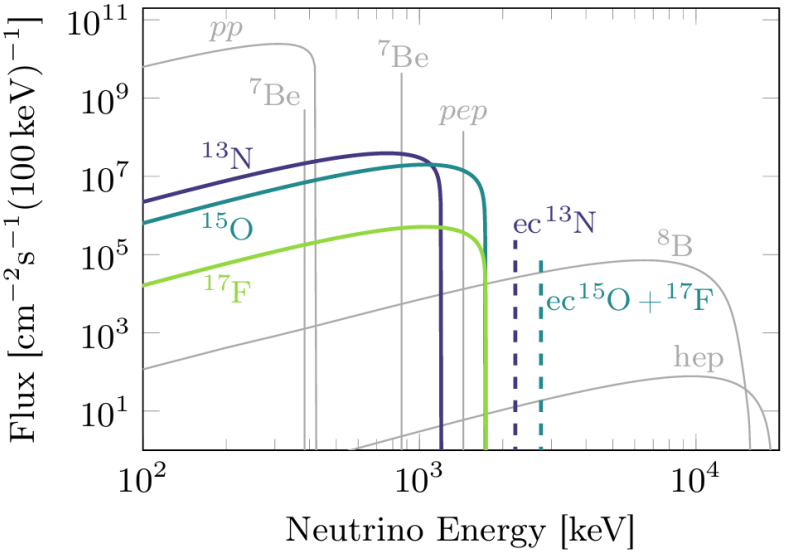

Figure 1.3: Energy spectra of solar neutrinos from the pp chain (in grey) and the CNO cycle (in colour). For mono-energetic lines the flux is given in $s^{-1}cm^{-2}$ [4].

In figure 1.3 we can see that the neutrino flux of the pp chain, which is dominant with respect to the CNO cycle as the latter occurs at higher temperatures, spans over smaller neutrino energies compared to the flux of the CNO cycle.

1.3.2 Supernovae and galactic sources

Core-collapse supernovae (CCSNe) are among of the most intense neutrino sources in our galaxy. They occur when stars of mass $M > 8M_{\odot}$ reach the end of their lifespan. Such massive stars are capable of burning Carbon nuclei, generating increasingly heavier elements, until the core is made up of Fe-peak elements. At this point, the stars have an "onion-like" structure, producing energy through fusion reactions is no longer possible. The electrons start to be captured by the Iron-group elements and then, due to nuclei photo-disintegration, by free protons.

$$p + e^{-} \rightarrow n + \nu_e \tag{1.8}$$

The capture described in equation 1.8 happens because the electrons energy is larger than the mass difference between neutrons and protons. This process starts the gravitational collapse: the extremely dense core becomes opaque to the produced neutrinos, forcing them to interact with the surrounding matter (known as neutrino trapping). Eventually, the neutrons in the core enter a degenerate state of matter, the collapsing core comes then to an abrupt halt, rebounding and producing a shockwave on impact with the external layers: material is ejected outward along with the trapped neutrinos. The duration of this last burst of immense energy can be calculated using the following expression for the neutrino mean free path:

$$\lambda = \frac{1}{\rho\sigma} \approx 10\,\mathrm{m} \tag{1.9}$$

where $\rho \sim 10^{38}$ nucleons $\times$ cm^{-3} and $\sigma \sim 10^{-41}$ cm^2 are the orders of magnitude of respectively the proto-neutron star density and the typical cross-section. Given the radius R of the proto-neutron star we can then calculate the neutrino diffusion time as follows:

$$\tau \sim \frac{\lambda}{c}\left(\frac{R}{\lambda}\right)^2 \sim 10\,\mathrm{s} \tag{1.10}$$

On February 1987, the then neutrino detectors revealed such event in the Large Magellanic Cloud (LMG), a satellite galaxy of the Milky Way:

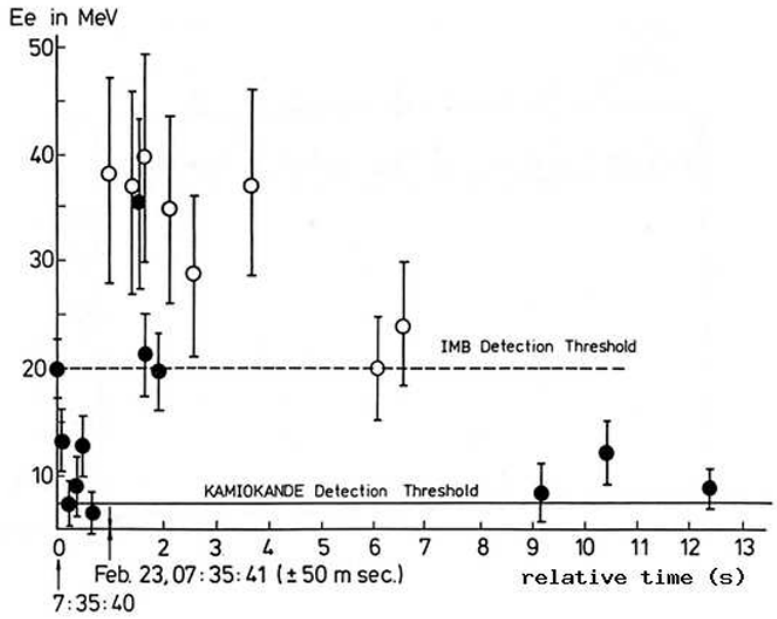

Figure 1.4: Energy of the cosmic events detected by Kamiokande II (closed circles) and IMB (open circles), produced by the SN1987A event, as a function of time in seconds [5].

In figure 1.4 we can appreciate the energy distribution and the time duration, approximately equal to 13 s, of the neutrino burst from the SN1987A event.

1.3.3 Extragalactic sources

The best candidates as extragalactic neutrino sources are the active galactic nuclei (AGNs). AGNs are compact regions in the center of galaxies emitting radiation that is fundamentally powered by dust accretion onto SMBHs. They are mainly divided into two classes: Seyfert galaxies, with a well visible host galaxy, and Quasars (QSOs), with no or a hardly visible host galaxy; both can be radio loud or quiet depending on whether they are jetted or not.

GRBs on the other hand are short and intense impulse of collimated γ-rays. They classify in short-bursts (sGRBs) and long-bursts (lGRBs) based on their T90 parameter, defined as the time interval over a burst emits from 5% to 95% of its total measured counts. sGRBs originate from the merger of binary neutron stars while lGRBs are due to hypernovae, the final stage of the gravitational collapse of stars massive enough ($M > 25M_{\odot}$) to form a black hole. Even if GRBs have been good candidates as sources

of high energy neutrinos for a long time, so far results form the ANTARES and IceCube telescopes did not show evidences of a correlation between GRBs and neutrinos.

Relativistic jets from AGNs are often associated with radio emissions and GRBs. In particular, AGNs with jets directed towards an observer are called blazars. As these objects are easier to spot and so to study, given their space orientation, hypotheses about the production of neutrinos in AGNs have been made possible.

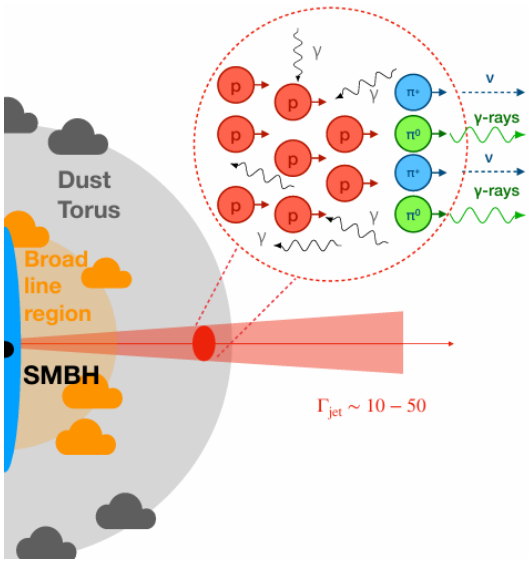

Figure 1.5: Schematic representation of neutrino production in a blazar relativistic jet. The Lorentz factor of the jet is indicated with Γ_{jet} [6].

Neutrinos are either produced in photo-pion ($p\gamma$) interactions [6]:

$$p + \gamma \rightarrow \pi^+ + n \tag{1.11}$$

or hadronic (pp) interactions:

$$p + p \rightarrow X + N_\pi \pi^\pm \tag{1.12}$$

where N_π is the pion multiplicity. Charged pions decay then by [7]:

$$\pi^+ \rightarrow \mu^+ + \nu_\mu \tag{1.13}$$

$$\pi^- \rightarrow \mu^- + \overline{\nu}_\mu \tag{1.14}$$

As blazars generate strong radiation fields surrounding protons are accelerated, making of the $p\gamma$ processes the prevalent processes; the pp processes can occur, for example, if a dust cloud intersect the accelerated protons. The resulting astrophysical neutrinos generally have energies slightly under the PeV unit.

Chapter 2

KM3NeT

In order to detect and retrieve the information carried by astrophysical messengers, detectors make use of a dielectric material, like water or ice, to achieve a phenomenon known as Cherenkov effect. As previously discussed, interactions between neutrinos and matter happen rarely: to increase the probability of such events to take place these telescopes should cover a volume large enough to make neutrino–nucleon processes significant.

The KM3NeT project (Cubic Kilometer Neutrino Telescope) is among the most recent series of detectors. Currently under construction in the Mediterranean Sea, it consists of two distinct detectors: KM3NeT/ORCA (Oscillation Research with Cosmics in the Abyss), located off the coast of Capo Passero, Sicily, and KM3NeT/ARCA (Astroparticle Research with Cosmics in the Abyss), located instead off the coast of Toulon.

Both of them are organized in building blocks of 115 detection units (DUs):

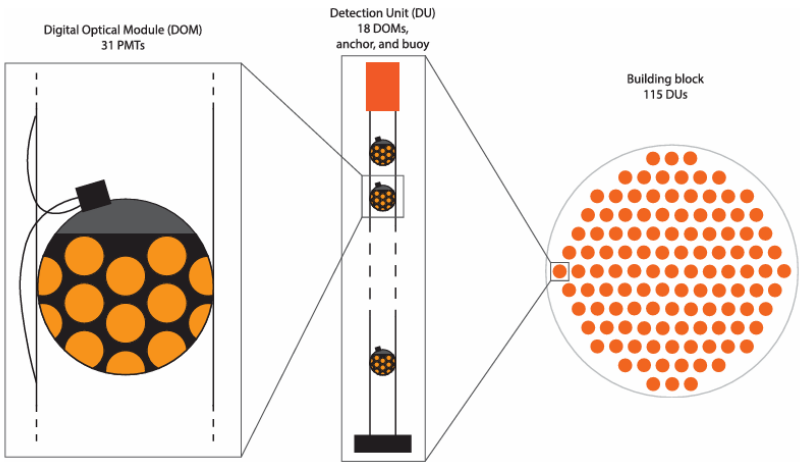

Figure 2.1: The KM3NeT full detector layout [8].

As shown in figure 2.1 each DU is composed of 18 digital optical modules (DOMs), spheres 44 cm in diameter, coated in a pressure-resistant glass and comprehensive of 31 photomultiplier tubes (PMTs). Such configuration offers a larger overall photocathode area with respect to previous-generation neutrino telescopes like ANTARES [9], resulting in improved spatial and temporal resolutions.

Figure 2.2: Rendering of a KM3NeT DOM with bollards attached to mechanically supporting cables in the deep-sea. In the cut out, the interior of the module with PMTs and electronics is visible [10].

The building blocks receives power supply and transmits data through electro-optical cables, in particular each DU sends the DOM information to 5 different junction boxes, implying the usage of the majority of the cables involved; in figure 2.2, the black breakout box of the DOM connects to the electro-optical network. The voltage of the PMTs required to increase the signal amplification factor in order to achieve the detection of Cherenkov radiation is about 1kV; if the minimum threshold of photoelectrons is reached, each of those signals will be converted into 6 bytes of data [11].

2.1 KM3NeT/ORCA and KM3NeT/ARCA

The KM3NeT detectors serve different purposes, therefore despite having similar fundamental layouts they turn out to be optimized for certain energy intervals.

KM3NeT/ORCA specialize in low-energy (MeV to TeV) neutrinos detection, whose creation is due to interactions with the atmosphere. KM3NeT/ORCA measurements are primarily intended for the study of the neutrino oscillation phenomenon and the mass hierarchy problem. Full detector will have one building block spanned over a volume of 0.067 km^3, with DUs 20 m apart from each other and a height of 200 m; DOMs are spaced at intervals of 9 m.

On the other hand, KM3NeT/ARCA is optimized for high-energy neutrinos detection, whose origin is traced back to astrophysical sources. Full detector will have two building block spanned over a volume of 1 km^3, well above that of KM3NeT/ORCA, with DUs 100 m apart from each other and a height of 700 m; DOMs are spaced at intervals of 36 m [11].

2.2 Neutrino detection

2.2.1 Cherenkov effect

Any working neutrino telescope collects the photons generated via Cherenkov effect. As charged particles pass through a dielectric transparent material, in the event that their velocity exceeds that of the light in the medium, molecules along their paths become polarized; an overall dipole momentum is created. Once the polarized molecules restore themselves to equilibrium a coherent radiation (Cherenkov radiation) is emitted with a characteristic angle θ_C (Cherenkov angle).

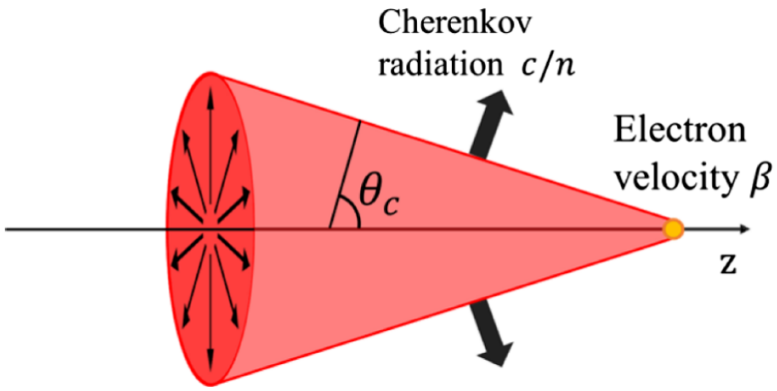

Figure 2.3: Schematic representation of the Cherenkov effect [12].

Figure 2.3 illustrates the process presented above. The Cherenkov angle is defined by the following relation:

$$cos(\theta_C) = \frac{1}{\beta n} \tag{2.1}$$

where β is the ratio of v (velocity of the particle) to c and n is the refractive index of the medium. For relativistic particles ($\beta \approx 1$) in seawater ($n \approx 1.364$) one finds that $\theta_C \approx 43°$.

The number N of Cherenkov photons emitted in the wavelength interval $d\lambda$, per unit of distance dx by a particle of charge e is given by the Frank-Tamm formula:

$$\frac{d^2N}{d\lambda dx} = \frac{2\pi}{137\lambda^2}\left(1 - \frac{1}{\beta^2 n^2}\right) \tag{2.2}$$

with λ being the Cherenkov radiation wavelength. From relation 2.2 it can be observed that the number of Cherenkov photons increases at smaller wavelengths. The optimal wavelength range for light propagation in seawater lies between 350 nm and 550 nm: KM3NeT PMTs are designed to reach maximum quantum efficiency within this interval [13].

2.2.2 Event classification

The secondary particles produced by neutrinos interacting with matter travel through the medium until they undergo processes with the latter or spontaneously decay. The mean distance traveled by these charged particles, the so-called *path length*, is a function of the particles energies.

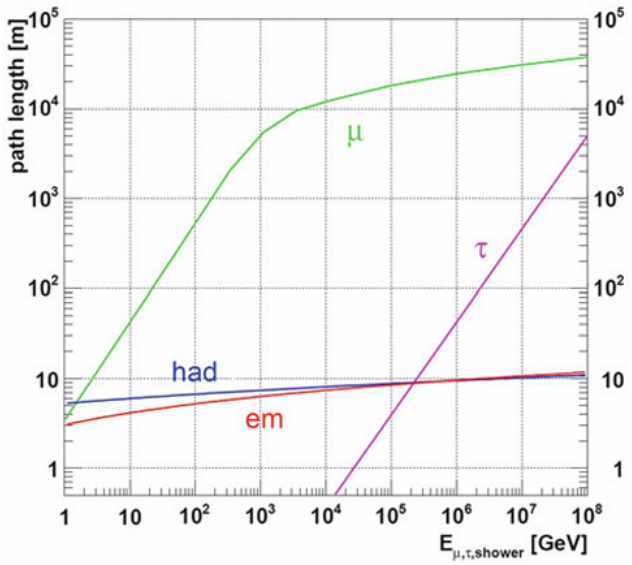

Figure 2.4: Path length of particles produced by neutrino interactions in water: muon (μ), tau (τ), electromagnetic (em) and hadronic (had) events versus their respective energy [14].

Figure 2.4 refers to shower events, characterized by the production of a large number of particles due to the decays of leptons. Events for which the trajectories of charged leptons can be resolved are called track events.

Shower events

Shower events are mediated predominantly by pion CC and NC interactions. NC processes only generate hadronic or electromagnetic (with the decay of the π^0 pion) showers. Both suffer from a large energy error as part of the interaction energy is always carried away by the outgoing neutrino, being a decay product. In particular, hadronic cascades are subject to fluctuations which are much more important with respect to electromagnetic ones. Muons, resulting from charged pion decay (dominant hadronic particle), produce long tracks, contributing substantially to the fluctuations.

A high energy electron resulting from a CC ν_e process has a high probability of radiating a photon via bremsstrahlung, which in turn would produce a $e^- e^+$ pair and consequently give rise to an electromagnetic shower. The latter has a length, defined as the distance within which 95% of the total energy has been distributed, in seawater of $\sim$ 10 m, being much smaller then the distance between the DUs of the KM3NeT telescopes. Therefore, pointing accuracy of shower events happens to be largely inferior.

For a CC ν_τ interaction, the resulting τ particle travels from a few meters up to a few kilometers before decaying and producing a second shower. The Cherenkov radiation emitted by the charger particle involved in the process is detect only if both ν_τ and τ interactions occur within the instrumental volume. The signature that results if they can be distinguished from each other is called *double bang event*. Alternatively, the signature for the τ lepton starting or ending outside of the instrumental volume is called *lollipop event* [13].

Track events

Track events are mostly given by CC ν_μ processes. The latter constitute a particularly important method for the search of cosmic point sources of neutrinos with energies larger than $\sim$ 1 TeV. Within this range the produced muons are typically energetic enough to traverse the detector in its entirety, resulting in distinct experimental signals which allow to accurately reconstruct the direction of the initial muon neutrino. The average angle $\theta_{\nu\mu}$ between the primary ν_μ and the outgoing μ satisfy the relation:

$$\theta_{\nu\mu} \leq \frac{0.6^\circ}{\sqrt{E_\nu[\mathrm{TeV}]}} \tag{2.3}$$

whit E_ν being the muon neutrino energy. CC ν_τ interactions can also be perceived as track events if the energy of the τ lepton is $\sim$ 1 PeV [13].

2.3 Background

2.3.1 Atmospheric muons and neutrinos

High-energy cosmic rays interactions with the Earth's atmosphere produce a particle shower mostly composed of either positive and negative pions. The latter decay according to either equation 1.13 or equation 1.14.

Progressively, the produced muons may decay in turn, according to the Feynman diagram presented in figure 1.1. Overall the number of muon neutrinos is about double the number of electron neutrinos, tau neutrinos are almost absent. These accidental atmospheric particles determine a part of the background noise observed by underwater telescopes.

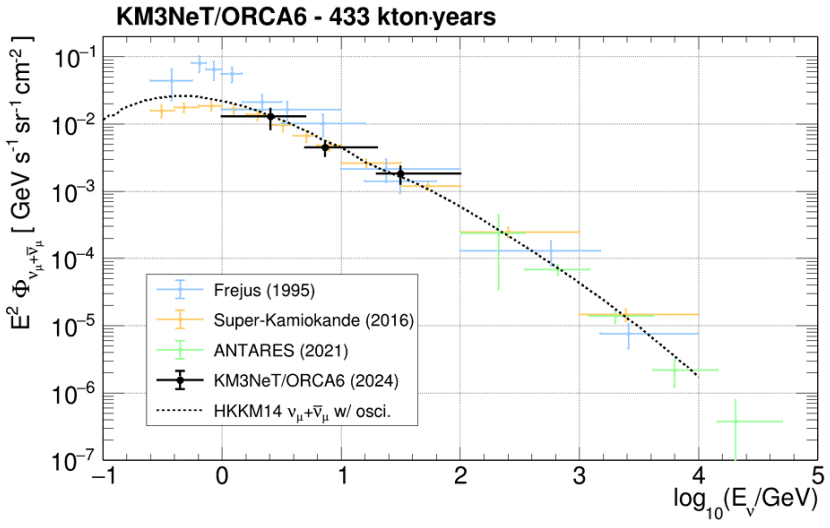

Figure 2.5: The atmospheric muon neutrino flux measurement with KM3NeT/ORCA6 compared to measurements from other experiments [15].

According to figure 2.5, the atmospheric muon neutrino flux decreases progressively at high energies, despite having a non-zero probability of passing through the Earth beneath.

Regarding the atmospheric muons, as they are unable to pass through the Earth, to exclude them one can consider the *upgoing* events only, produced in the hemisphere opposite to the detector.

2.3.2 Radioactive isotopes and bioluminescence

Dissolved in seawater, small quantities of radioactive isotopes are present, the most abundant of which is Potassium-40 (^{40}K). It undergoes β-decay via either one of the two following reactions:

$$^{40}K \rightarrow \ ^{40}Ca \ + \ e^{-} + \overline{\nu}_e \tag{2.4}$$

$$^{40}K \ + \ e^{-} \rightarrow \ ^{40}Ar \ + \ \nu_e \ + \ \gamma \tag{2.5}$$

The majority of the electrons produced by equation 2.4 fall over the energy threshold demanded to produce Cherenkov radiation. Photons due to equation 2.5 are energetic enough to bring the remaining electrons over the threshold via Compton scattering.

A substantial part of the measured optical background resides in bioluminescence phenomena, carried out by deep-sea organisms and bacteria. Their emission spectra are centered around a wavelength of 470-480 nm.

Although signals that derive from bacteria represent a larger portion of the overall bioluminescence optical background, they are negligible below a certain depth.

Ultimately, bioluminescence signals prove difficult to predict, as they fluctuate significantly with the time of year, the velocity of marine currents, and the geographic location [13].

Chapter 3

Comparison between the performances of KM3NeT/ORCA and KM3NeT/ARCA

This work discusses the detector performances of KM3NeT/ORCA and comparison with KM3NeT/ARCA by looking at key parameters in the context of astronomy analyses. The KM3NeT/ORCA18 configuration, for KM3NeT/ORCA, and the KM3NeT/ARCA21 configuration, for KM3NeT/ARCA, have been considered, due to their similar number of lines and data-taking livetime.

Key performance criteria include the muon contamination, the energy and angular resolution and the effective area. The signal and background expectations are based on Monte Carlo (MC) simulations of reconstructed KM3NeT events from which fundamental detector parameters can be retrieved.

The detector performances are presented for two sets of cuts:

- Minimum cut selections, in order to ensure a correct reconstruction of the events. For KM3NeT/ORCA18, these cuts consist of an *upgoing* selection of events, reconstructed as tracks, along with an *antinoise* selection, intended to reduce spurious signals and background not consistent with real neutrino interactions.

- Cut selections, established by the KM3NeT collaboration, concerning parameters that indicate the quality of the reconstruction fit. They have been used to define the sample employed in searches for point-like sources of cosmic neutrinos (PS cuts). These cut selections are specified, for KM3NeT/ORCA18, as BDT selections, trained to determine whether a certain event belongs to the background or not. For the KM3NeT/ARCA21 configuration, they are defined taking into account the likelihood, track length and uncertainty in the reconstructed track direction.

3.1 Muon contamination

As discussed previously in subsection 2.3.1, detectors are affected by background due to atmospheric particles like muons. The graphs below show the muon contamination in the total amount of selected MC events as a function of the reconstructed energy. Such collection of events, hereafter referred to as MC SUM, includes cosmic neutrinos, atmospheric neutrinos and muons.

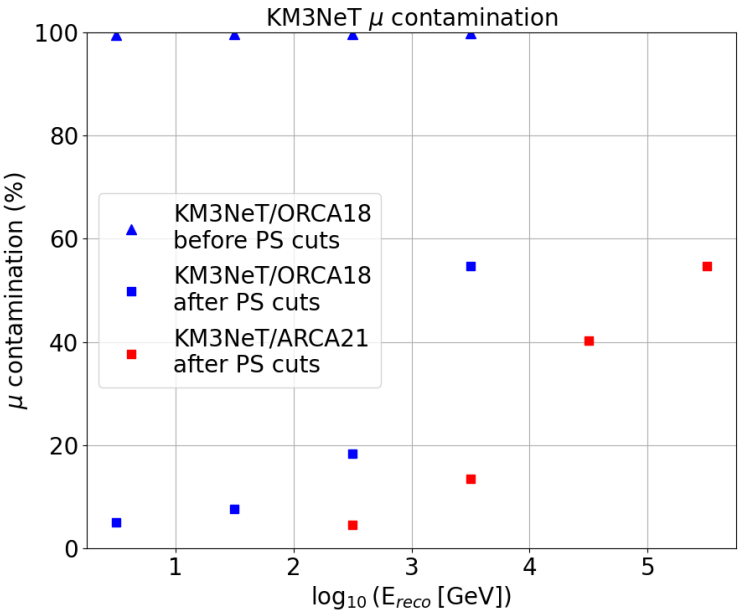

Figure 3.1: Muon contamination affecting KM3NeT/ORCA18 and KM3NeT/ARCA21 as a function of the logarithm of the reconstructed energy and expressed as a percentage of MC SUM. After PS cuts case is depicted for both KM3NeT/ORCA18 and KM3NeT/ARCA21, while before PS cuts case is shown only for KM3NeT/ORCA18.

After the PS cuts have been applied, the number of muons drastically decreases, especially at lower energies. The percentage of the number of muons over the whole considered energy range with respect to the total number of all types of events is indeed $< 10\%$ for KM3NeT/ORCA18 and $< 16\%$ for KM3NeT/ARCA21.

In table 3.1, values of KM3NeT/ORCA18 key quantities for muon contamination are reported.

KM3NeT/ORCA18	**Analysis**	**Value**	**Particle**	**Events**
Before PS cuts	μ contamination (%)	99.6%	$E^{-2}\ \nu_{cos}$	0.38
			ν_{atm}	3376.2
			μ_{atm}	839994.6
After PS cuts	μ contamination (%)	9.9%	$E^{-2}\ \nu_{cos}$	0.3
			ν_{atm}	3025.6
			μ_{atm}	331.3

Table 3.1: KM3NeT/ORCA18 muon contamination values in both PS cuts cases. The number of detected cosmic neutrinos, atmospheric neutrino and atmospheric muons for a E^{-2} spectrum are also shown.

In all of the plots presented below, the respective PS cuts are applied to select the KM3NeT/ORCA and KM3NeT/ARCA events.

3.2 Energy Resolution

The precision with which the energy of the simulated events is reconstructed is described by the energy resolution.

The following 2-dimensional histograms show the cosmic neutrino distribution of true versus reconstructed energy for KM3NeT/ORCA18 and KM3NeT/ARCA21 for both E^{-2} and E^{-3} energy spectrum, as the cosmic neutrino flux is parametrized as:

$$\Phi(E) = \Phi_0 E^{-\gamma} \tag{3.1}$$

with γ being the spectral index and Φ_0 the flux normalization.

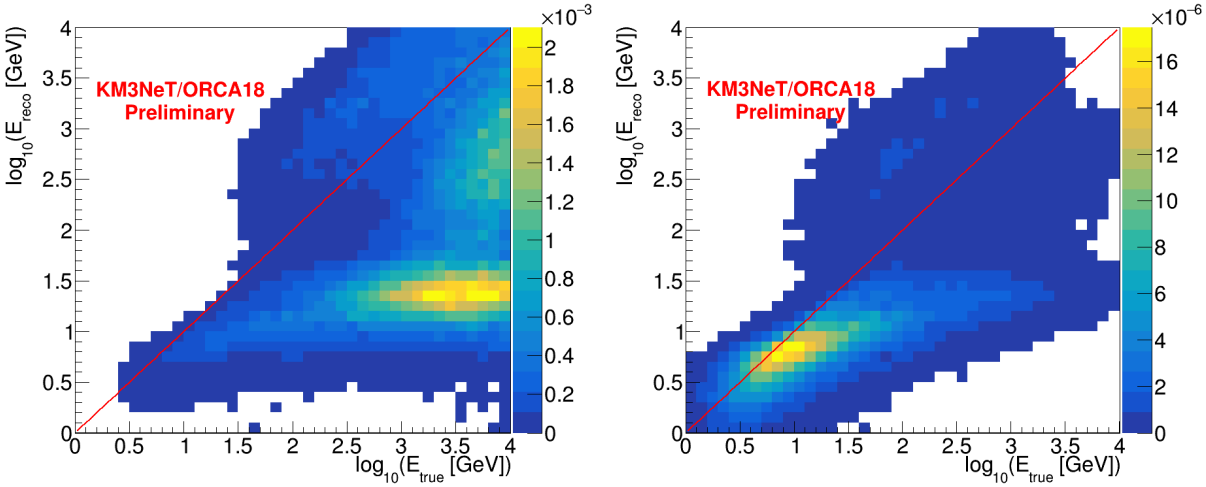

Figure 3.2: Reconstructed energy as a function of true neutrino energy for cosmic neutrinos for KM3NeT/ORCA18, for a E^{-2} spectrum (left), and KM3NeT/ORCA18, for a E^{-3} spectrum (right). The color scale indicates the bin contents.

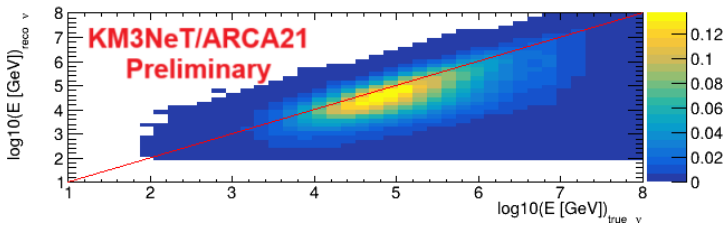

Figure 3.3: KM3NeT/ARCA21, for a E^{-2} spectrum. The latter belongs to an internal note of the KM3NeT collaboration and it is not part of this work. The color scales index the contents of the bins.

The distributions in figure 3.2 take into account all cosmic events $\nu_f + \overline{\nu}_f$, with $f \in \{e,\ \mu,\ \tau\}$.

A noticeable difference can be observed between the two plots of KM3NeT/ORCA18 for a E^{-2} and E^{-3} energy spectrum respectively. In particular, this shows that a significantly better agreement between true and reconstructed energy is achieved for lower energy events. The distribution in figure 3.3 is displayed for comparison.

The plots presented in the following sections refer to a E^{-2} energy spectrum.

3.3 Effective Area

Another important quantity used to describe the performance of the detector resides in its effective area. It is the equivalent area of an ideal detector with 100% detection efficiency.

The effective area A_ν^{eff} is defined by the following equation [13]:

$$A_\nu^{eff}(E_\nu) = P_{\nu\mu}(E_\nu, E_{thr}^\mu) \cdot A \cdot e^{-\sigma(E_\nu)\rho N_A Z(\theta)} \tag{3.2}$$

where, for the term $e^{-\sigma(E_\nu)\rho N_A Z(\theta)}$, $\sigma(E_\nu)$ is the total neutrino-nucleon cross section, with E_ν being the neutrino energy, N_A the Avogadro number, (ρN_A) the target nucleon density, θ the neutrino direction with respect to the nadir and $Z(\theta)$ the Earth path. A corresponds to the detector area and $P_{\nu\mu}(E_\nu, E_{thr}^\mu)$ represents the probability that a neutrino with energy E_ν produces a muon of energy E_μ which survives with energy $> E_{thr}^\mu$, after the propagation from the interaction point to the detector.

The effective area of KM3NeT/ORCA18 for each leptonic flavour is displayed in the figure 3.4 as a function of the true neutrino energy. A comparison between the effective area of KM3NeT/ORCA18 and KM3NeT/ARCA21 for all neutrino flavours is also shown.

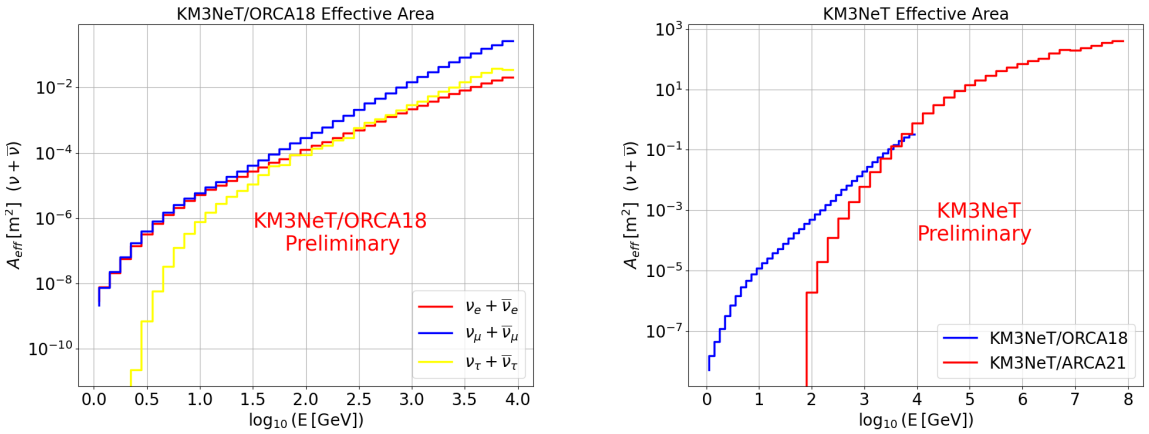

Figure 3.4: Effective area of KM3NeT/ORCA18 as a function of the true neutrino energy for different leptonic flavours (left) and comparison between KM3NeT/ORCA18 and KM3NeT/ARCA21 for all neutrino flavours (right).

In figure 3.4 (right) the effective area of KM3NeT/ORCA18 and KM3NeT/ARCA21 are noticeably different from each other. This is due to different spacings within the two detectors.

3.4 Angular Resolution

A crucial performance criterion when it comes to astronomy analyses relies in the reconstruction precision of cosmic neutrino direction. The angular resolution of a detector is defined as the angle subtended by the true and reconstructed direction. This angle depends on the intrinsic kinematic angle, that lies between the incoming neutrino and the outgoing muon, on detector-related properties, in particular light scattering of the medium in which the detector is placed and the geometry of the detector and also on the performance of the reconstruction algorithm.

The subsequent plots show the median and 68% containment values, corresponding to 1σ confidence level, of the angular resolution for $\nu_\mu + \overline{\nu}_\mu$ cosmic events. A comparison between KM3NeT/ORCA6, a previous configuration of KM3NeT/ORCA, and KM3NeT/ORCA18 has been performed, as well as a comparison between the latter and KM3NeT/ARCA21.

A 1-dimensional angular distribution, for the KM3NeT/ORCA18 configuration, normalized by the dataset livetime is also shown.

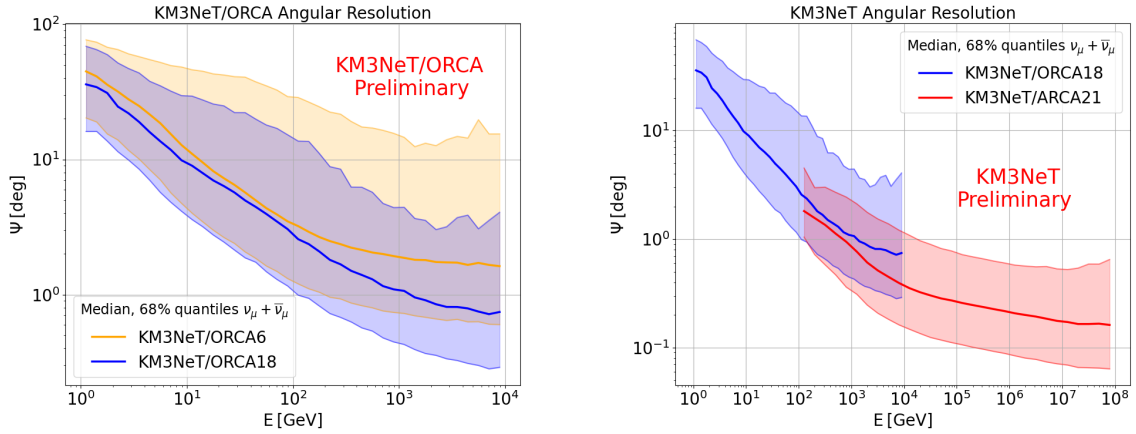

Figure 3.5: Comparison of the angular resolution as a function of the true neutrino energy, between KM3NeT/ORCA6 and KM3NeT/ORCA18 (left) and between KM3NeT/ORCA18 and KM3NeT/ARCA21 (right). A log-scaled energy axis has been set up.

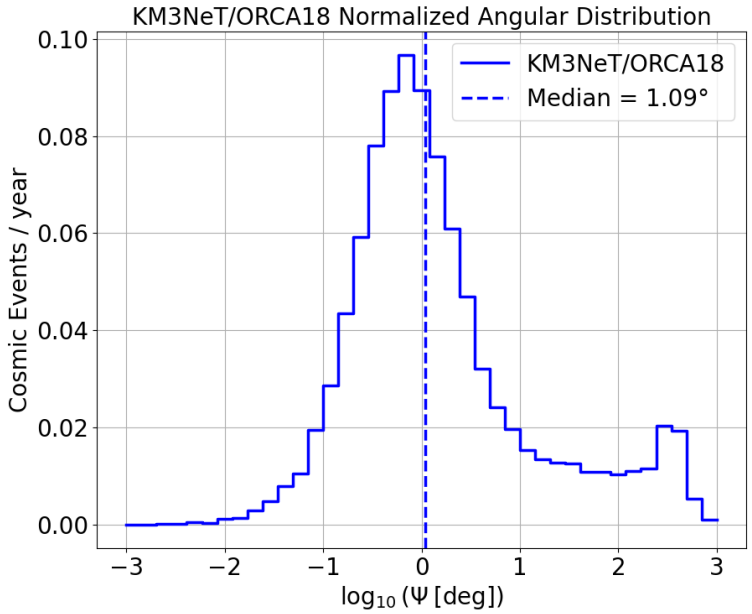

Figure 3.6: 1-dimensional angular resolution for KM3NeT/ORCA18 for ν_μ CC events.

Conclusions

PS cuts permit to reduce significantly the muon contamination, which however remains relatively high in both of the detectors at the at higher energies.

At greater energies key parameters including the effective area and the angular resolution improve. Thus, neutrino detectors are optimized for astronomy analyses at the latest parts of the energy spectra.

A noticeable improvement of the detector performances regarding the angular resolution for increasing numbers of KM3NeT/ORCA lines is observed. This parameter improves significantly for larger detectors, which leads to a greater detected fraction of a track. Moreover, the angular resolution of KM3NeT/ORCA is comparable at that of KM3NeT/ARCA between 100 GeV and 10 TeV; within this interval a similar or greater A_{eff} is also provided by KM3NeT/ORCA.

The KM3NeT/ORCA detector is particularly promising for extending astronomy analyses at lower energies.

Bibliography

[1] Edoardo Vitagliano, Irene Tamborra, and Georg Raffelt. "Grand unified neutrino spectrum at Earth: Sources and spectral components". In: *Reviews of Modern Physics* 92.4 (Dec. 2020). ISSN: 1539-0756. DOI: 10.1103/revmodphys.92.045006. URL: http://dx.doi.org/10.1103/RevModPhys.92.045006.

[2] Bruce T. Cleveland et al. "Measurement of the Solar Electron Neutrino Flux with the Homestake Chlorine Detector". In: *The Astrophysical Journal* 496.1 (Mar. 1998), p. 505. DOI: 10.1086/305343. URL: https://dx.doi.org/10.1086/305343.

[3] Maurizio Spurio. *Neutrini in profondità: Vita, morte e miracoli dei neutrini rivelati sotto terra, sotto i ghiacci o in fondo al mare*. 2016. arXiv: 1609.06710 [physics.hist-ph]. URL: https://arxiv.org/abs/1609.06710.

[4] "Experimental evidence of neutrinos produced in the CNO fusion cycle in the Sun". In: *Nature* 587.7835 (Nov. 2020), pp. 577–582. ISSN: 1476-4687. DOI: 10.1038/s41586-020-2934-0. URL: http://dx.doi.org/10.1038/s41586-020-2934-0.

[5] I. Leonor et al. "Searching for prompt signatures of nearby core-collapse supernovae by a joint analysis of neutrino and gravitational-wave data". In: *Classical and Quantum Gravity* 27 (Feb. 2010). DOI: 10.1088/0264-9381/27/8/084019.

[6] Foteini Oikonomou. *High-Energy Neutrino Emission from Blazars*. 2022. arXiv: 2201.05623 [astro-ph.HE]. URL: https://arxiv.org/abs/2201.05623.

[7] Douglas Bryman and Robert Shrock. *Pion Decay*. 2025. arXiv: 2502.18384 [hep-ph]. URL: https://arxiv.org/abs/2502.18384.

[8] S. Aiello et al. "Astronomy potential of KM3NeT/ARCA". In: *The European Physical Journal C* 84.9 (Sept. 2024). ISSN: 1434-6052. DOI: 10.1140/epjc/s10052-024-13137-2. URL: http://dx.doi.org/10.1140/epjc/s10052-024-13137-2.

[9] A. Albert et al. "The ANTARES detector: Two decades of neutrino searches in the Mediterranean Sea". In: *Physics Reports* 1121-1124 (2025), pp. 1–46. ISSN: 0370-1573. DOI: https://doi.org/10.1016/j.physrep.2025.04.001. URL: https://www.sciencedirect.com/science/article/pii/S0370157325001450.

[10] KM3NeT Collaboration. *The KM3NeT multi-PMT optical module*. 2022. arXiv: 2203.10048 [astro-ph.IM]. URL: https://arxiv.org/abs/2203.10048.

[11] KM3NeT Collaboration. URL: https://www.km3net.org.

[12] Yuichi Tadenuma et al. "Generation of coherent THz Cherenkov radiation by electron bunch tilt control". In: *Phys. Rev. Accel. Beams* 25 (11 Nov. 2022), p. 110102. DOI: 10.1103/PhysRevAccelBeams.25.110102. URL: https://link.aps.org/doi/10.1103/PhysRevAccelBeams.25.110102.

[13] T. Chiarusi and M. Spurio. "High-energy astrophysics with neutrino telescopes". In: *The European Physical Journal C* 65.3–4 (Jan. 2010), pp. 649–701. ISSN: 1434-6052. DOI: 10.1140/epjc/s10052-009-1230-9. URL: http://dx.doi.org/10.1140/epjc/s10052-009-1230-9.

[14] Maurizio Spurio. *Probes of multimessenger astrophysics: Charged cosmic rays, neutrinos, Y-rays and gravitational waves*. Springer, 2018.

[15] KM3NeT Collaboration. *Measurement of the atmospheric ν_μ flux with six detection units of KM3NeT/ORCA*. 2025. arXiv: 2504.09119 [hep-ex]. URL: https://arxiv.org/abs/2504.09119.